WILEY InterScience® DISCOVER SOMETHING GREAT

Assessment of natural and synthetic wollastonite as source for bioceramics preparation

R. G. Carrodeguas,[1] A. H. De Aza,[2] P. N. De Aza,[3] C. Baudín,[2] J. Jiménez,[4] A. López-Bravo,[4] P. Pena,[2] S. De Aza[2]

[1]*Centro de Biomateriales, Universidad de La Habana, Ave. Universidad s/n e/G y Ronda, Apdo. Postal 6130, 10600, La Habana, Cuba*

[2]*Departamento de Cerámica, Instituto de Cerámica y Vidrio, Consejo Superior de Investigaciones Científicas (CSIC), Campus de Cantoblanco, Calle Kelsen 5, 28049 Madrid, Spain*

[3]*Instituto de Bioingeniería, Universidad Miguel Hernández, Avenida Universidad s/n, Edif. Vinalopó, 03202 Elche, Alicante, Spain*

[4]*Hospital Provincial de Ávila, C/ Jesús del Gran Poder 42, 05003 Ávila, Spain*

Received 8 September 2006; accepted 27 November 2006
Published online 14 May 2007 in Wiley InterScience (www.interscience.wiley.com). DOI: 10.1002/jbm.a.31216

Abstract: Pseudowollastonite ceramics (β-$CaSiO_3$) from synthetic and natural sources were assessed with regard to their properties relevant to biomedical applications. Synthetic and natural $CaSiO_3$ powders, with average particle size of 1.6 and 13.2 μm, respectively, were first employed. Powders were pressed and sintered at 1400°C for 2 h. Pseudowollastonite was the only crystalline phase in sintered materials. Glassy phase, eight times more abundant in sintered natural wollastonite (SNW) than in the synthetic one (SSW), was observed in grain boundaries and in triple points. Larger grains and bigger and more abundant pores were present in SNW, resulting in lower diametral tensile strength (26 MPa), than in SSW (42 MPa). However, by milling the natural wollastonite starting powder to a particle size of 2.0 μm and sintering (SNW-M), the microstructure became finer and less porous, and diametral tensile strength increased (48 MPa). Weibull modulus of SNW and SNW-M samples was twice that of the SSW. All the samples released Si and Ca ions, and removed phosphate ions from simulated body fluid in similar amounts and were completely coated by apatite-like spherules after soaking in simulated body fluid for 3 wk. The aqueous extracts from all samples studied were not cytotoxic in a culture of human fibroblastic cells. No differences in fibroblast-like human cells adhesion and proliferation were observed between samples. According to the obtained results, properly processed pseudowollastonite bioceramics, obtained from the natural source, exhibit the same *in vitro* behavior and better performance in terms of strength and reliability than do the more expensive synthetic materials. © 2007 Wiley Periodicals, Inc. J Biomed Mater Res 83A: 484–495, 2007

Key words: wollastonite; mechanical properties; *in vitro* test; cytotoxicity; cell adhesion

INTRODUCTION

Glasses composed of SiO_2, Na_2O, CaO, and P_2O_5, which were developed by Hench et al., were the first materials where *in vitro* bioactivity and tight bond to living bone were observed.[1] After this, several phosphorus-containing materials have also been described as bioactive, which exhibit quite different nature. Apatite-wollastonite glass-ceramics from the system MgO-CaO-SiO_2-P_2O_5-CaF_2[2] and some calcium phosphate ceramics were soon established as bioactive materials, and they are currently used in clinical practice as fillers for bone defects, middle ear, vertebral, and dental implants.[3]

However, phosphorus-containing ceramics, bioglasses, and glass-ceramics are not the only bioactive materials. Ohura et al. also observed the formation of an apatite layer on the surface of glasses of the system CaO-SiO_2 exposed to a simulated body fluid (SBF).[4] More recently, synthetic crystalline compounds in the systems CaO-MgO-SiO_2 and CaO-SiO_2, for example, diopside ($CaMgSi_2O_6$) and pseudowollastonite (β-$CaSiO_3$), have also been found to be bioactive.[5–8] Pseudowollastonite ceramics quickly react in SBF. Calcium ions from the pseudowollastonite network are exchanged for H^+ from the SBF

Correspondence to: S. De Aza; e-mail: aza@icv.csic.es
Contract grant sponsor: Projects CICYT MAT2003-08331-C02-01 and 02
Contract grant sponsor: CYTED Network VIII.J "Biomateriales para la Salud"
Contract grant sponsor: National Program for Mobility of Foreign Researchers of the Ministry of Education and Science of Spain; contract grant number: SAB2005-0015

© 2007 Wiley Periodicals, Inc.

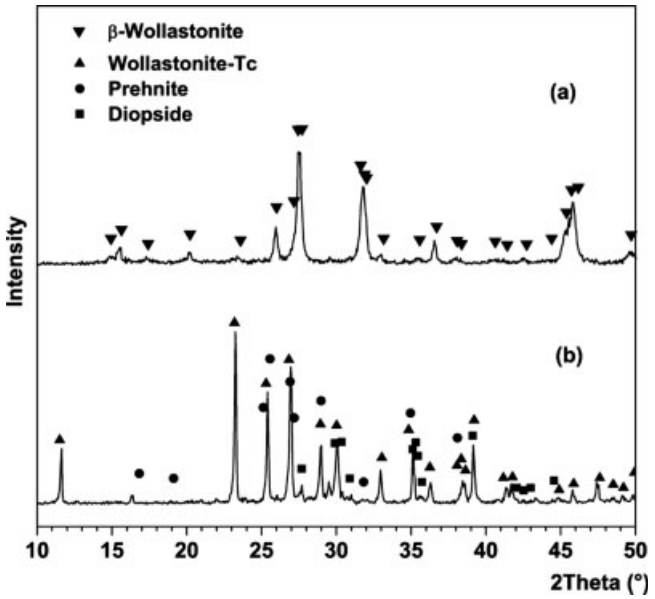

Figure 1. X-ray diffraction patterns of synthetic and natural wollastonite powders. (a) Synthetic; (b) Natural.

medium and an amorphous silica layer is formed. Because of this exchange, the pH, just at the interface pseudowollastonite/SBF, increases up to 10.5 and partial dissolution of the amorphous silica and precipitation on the pseudowollastonite surface of an apatite-like phase take place.[9] *In vivo* test in rat tibia showed that osteoblasts migrate to the surface of pseudowollastonite implants and deposit new woven bone directly onto their surface, which gradually transforms into mature bone.[10,11] Synthetic pseudowollastonite ceramic was not cytotoxic,[12] and on the contrary, dissolution products from pseudowollastonite ceramics induced calcification in osteoblast cultures *in vitro*.[13–15] In spite of the availability of high purity and cheap commercial natural wollastonite,[16] only synthetic pseudowollastonites have been studied and evaluated as precursors for preparing bioactive pseudowollastonite ceramics.

Thus, the present research is aimed to compare pseudowolllastonite ceramics from synthetic and natural sources with regard to their properties relevant to biomedical applications.

MATERIALS AND METHODS

Materials

Synthetic polycrystalline pseudowollastonite powder was prepared by solid state reaction between $CaCO_3$ (Probus AG) and SiO_2 (washed Belgian sand) in a molar ratio equal to 1, as elsewhere described, and grinded to an average particle size of 1.6 μm.[17] Powdered natural wollastonite, Vansil® W40, was supplied by R.T. Vanderbilt, with an average particle size of 13.2 μm. Part of this material was milled in isopropanol by attrition milling to an average particle size of 2.0 μm. Qualitative X-ray diffraction analysis showed that the major crystalline phase was β-$CaSiO_3$ (JCPDF 31-0300) in the synthetic powder and α-$CaSiO_3$, also called $CaSiO_3$-Tc (JCPDF 43-1460), in the natural one. Minor amounts of prehnite ($2CaO{\cdot}Al_2O_3{\cdot}3SiO_2{\cdot}H_2O$, JCPDF 29-0290) and diopside ($Ca(Mg,Al)_2(Si,Al)_2O_6$ JCPDF 41-1370) were also found in the natural wollastonite (Fig. 1).

The results of chemical analysis by X-ray fluorescence, for both materials, are shown in Table I.

Sintered ceramics were prepared by one of the following procedures:

a. Powders were axially pressed in a stainless steel mould at 500 MPa and sintered at 1400°C for 2 h, with heating and cooling rates of 600°C/h. Sintered cylinders were 4.0–5.0 mm in diameter and 3.2–3.6 mm in height.
b. Powders were isostatically pressed at 200 MPa and sintered as described earlier. Discs of 10 mm diameter and 1 mm thickness were cut with a diamond saw.

Hereafter, the terms SSW (sintered synthetic wollastonite), SNW (sintered natural wollastonite), and SNW-M will be employed to designate ceramics prepared from synthetic pseudowollastonite and from not-milled and milled natural wollastonite, respectively.

X-Ray diffraction

X-Ray diffraction analysis was performed on powdered specimens in a diffractometer D5000 with a Kristalloflex goniometer (Siemens) and Cu-target. Diffractograms were recorded employing Ni-filtered radiation ($\lambda = 1.5406$ Å), and anodic voltage and current of 50 kV and 30 mA, respectively. The step size was 0.05° and the time/step ratio was 1.5 s.

Microstructure characterization

The microstructure was studied on specimens polished with diamond down to 1 μm and chemically etched, when

TABLE I
Chemical Composition of the Starting Materials (wt %)

Component	Natural Wollastonite	Synthetic Pseudowollastonite
CaO (%)	44.3 ± 0.3	48.2 ± 0.3
SiO_2 (%)	50.1 ± 0.3	51.3 ± 0.3
Al_2O_3 (%)	0.75 ± 0.01	0.18 ± 0.01
MgO (%)	1.99 ± 0.01	0.13 ± 0.01
Na_2O (%)	0.24 ± 0.002	0.019 ± 0.002
K_2O (%)	0.069 ± 0.001	0.076 ± 0.001
MnO (%)	0.026 ± 0.003	0.029 ± 0.003
Fe_2O_3 (%)	0.14 ± 0.004	0.042 ± 0.004
TiO_2 (%)	0.019 ± 0.002	n.d.
SrO (%)	0.041 ± 0.002	0.013 ± 0.002
BaO (%)	0.043 ± 0.002	n.d.
ZnO (%)	0.012 ± 0.002	n.d.
P_2O_5 (%)	0.077 ± 0.003	0.029 ± 0.003
SO_3 (%)	0.015 ± 0.002	n.d.
L.O.I. (%)	2.13 ± 0.03	n.d.
SiO_2/CaO (molar ratio)	1.056 ± 0.001	0.994 ± 0.008

required, with diluted acetic acid (1:5). Gold-coated samples were examined in the scanning electron microscope (SEM).

Scanning electron microscopy and energy dispersive spectroscopy

SEM analysis was performed using a field emission scanning electron microscope Hitachi S-4700 (Hitachi, Japan). For elemental microanalysis and mapping, an X-Ray energy dispersive spectroscopy (EDS) module was employed coupled to the microscope. Samples were gold coated, except those intended to phosphorus microanalysis or mapping, which were coated with graphite.

In vitro bioactivity

To assess *in vitro* bioactivity, discs, prepared by procedure b, were immersed in Kokubo's conventional Simulated Body Fluid[18] at 36.5°C using a ratio of volume of SBF to area of ceramic of 0.5 cm^3/mm^2. SBF was replaced every 2 days. Discs were removed at 1, 2, and 3 days, and 1, 2, and 3 wk of immersion, and rinsed with distilled water and acetone and let dry in air.

Ion release

The calcium, silicon, and phosphorus ions release profiles in SBF at 36.5°C were determined for SSW and SNW. Cylinders prepared by uniaxial pressing and sintering were immersed in Kokubo's conventional SBF[18] at 36.5°C, using a ratio of volume of SBF to area of ceramic of 0.5 cm^3/mm^2. The SBF was removed and replaced with a fresh portion after several periods of immersion. Calcium, silicon, and phosphorus were determined in the removed SBF by inductively coupled plasma atomic emission spectrometry.[12]

Ceramic/SBF interfacial pH

An ion-sensitive field-effect transistor (ISFET-Meter) of Si_3N_4 type[9] (built at the Centro Nacional de Microelectrónica CNM-CSIC, Universidad Autónoma de Barcelona. 08193 Bellaterra, Barcelona, Spain) was used to measure the pH exactly at the ceramic/SBF interface. A disc of the SNW-M sample prepared by the procedure b was clamped just onto the microelectrode and immersed in SBF solution at 37°C (Fig. 2). The pH was continuously monitored by means of a potentiometer, an X–Y recorder, and an Ag/AgCl reference electrode.

Diametral compression strength

Disc specimens fabricated by uniaxial pressing and sintering were used for strength determinations by Diametral Compression (DCDT), also known as Brazilian or Brittle Ring Test. This test was initially proposed for concretes[19,20] and has been proved to be a simple and practical method for measuring the tensile strength of brittle materials even

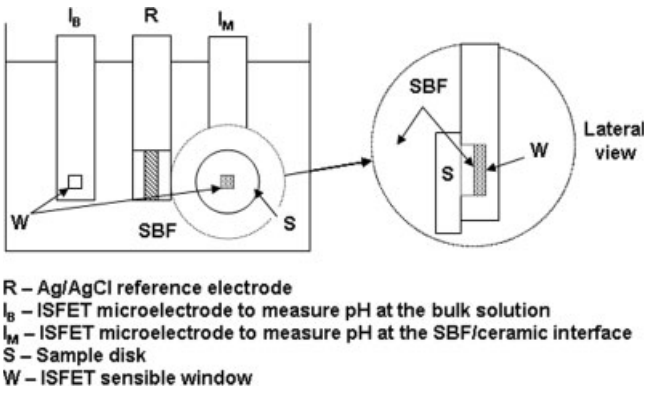

Figure 2. Scheme of the experimental device for interfacial pH measurement.

with relatively large amounts of porosity (30–60 vol %).[21] Specimens were placed between two stainless steel loading plates using carton pads to distribute load. Load was applied using 5 mm/min rate for the displacement of the loading frame in a universal testing machine (Microtest, Spain). Fifteen specimens of each composition were tested and the strengths were calculated using Eq. (1):

$$\sigma = 2P/\pi DT \quad (1)$$

where P is the applied load, and D and T are the diameter and the thickness of the disc, respectively.

DCDT is based upon the state of stress developed when a cylindrical specimen is compressed between two opposite generators of its surface. Maximum tensile stresses, proportional to the applied load, are developed normal to the loading direction across the diametrical plane of the specimen parallel to the loading direction. Fracture has to be initiated by these tensile stresses for the test to yield useful results and for Eq. (1) to be valid to calculate stress. Additional high shear and compressive stresses develop close to the ends of the specimen in contact with the loading plates, especially in high Young's modulus materials, that should be reduced if failure is to initiate in tension. Therefore, all fractured samples were analyzed to ensure that fracture was not originated by extensive local crushing close to the loading points.

Weibull reliability analysis

The distribution of strength values of brittle materials is well described by the Weakest Link Theory, which can be acceptably represented by the Weibull function.[22] The Weibull parameters were determined by the procedure of ENV-843-5. This standard implies the use of the simplest form of the Weibull function,[22] Eq. (2), where $P_f(\sigma)$ is the probability of failure at the stress σ, σ_0 is a scaling constant, also called characteristic strength, that corresponds to the stress at which the probability of failure is 63.2 %, and m is the Weibull modulus.

$$P_f(\sigma) = 1 - \exp\left(-\frac{\sigma^m}{\sigma_0^m}\right) \quad (2)$$

According to this standard, the probabilities of failure were calculated using Eq. (3):

$$P_f = \frac{n - 0.5}{N} \quad (3)$$

where N is the total number of specimens tested and n is the specimen rank in ascending order of failure stress. For this simple form of the Weibull function, the threshold stress below which no failure occurs in the material is taken as zero, as adequate for brittle ceramics. This Weibull function has been proven to describe adequately the strength distribution of porous materials (16–60 vol %).[20–23]

From a linear adjustment by the maximum likelihood method of the plot ln (ln $(1/(1-P_f))$ versus ln(σ_f), characteristic strength and Weibull modulus were estimated for each material. Upper and lower 90% confidence limits were calculated for the Weibull modulus and the characteristic strength to ensure significance of the results. The fracture surfaces of tested specimens were observed by SEM.

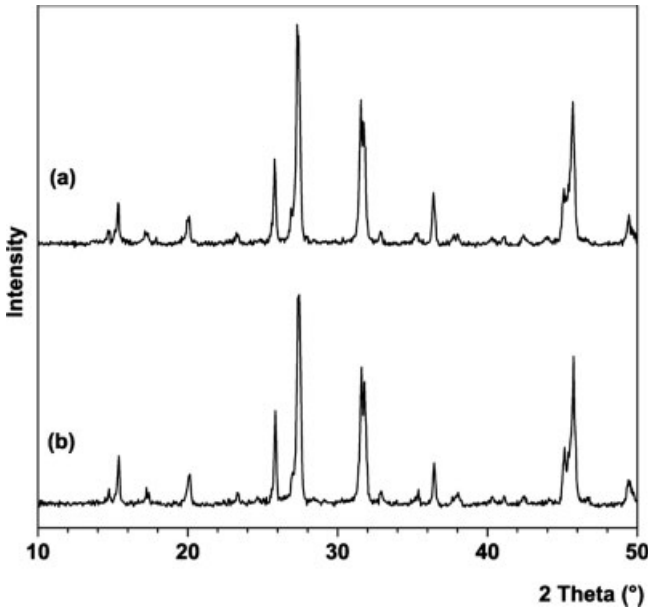

Figure 3. X-ray diffraction patterns of sintered wollastonites. (a) SSW; (b) SNW.

Indirect cytotoxicity by the 3-(4,5-dimethylthiazol-2-yl)-2,5-diphenyltetrazolium bromide (MTT) method

For indirect cytotoxicity assay (MTT method), discs of each material (10 mm diameter × 1 mm thickness), fabricated by isostatic pressing and sintering, were sterilized by ethylene oxide and submitted to indirect cytotoxicity test by the MTT method.[24] Thermanox (TMX) discs were used as negative control and a 0.5 wt/vol % solution of poly(ethyleneglycol octylphenyl ether) (Triton X-100, TTN) in the culture medium was the positive control. The cells employed were a primary cell culture of human fibroblasts. The culture medium was minimal essential medium Eagle (MEM), modified with HEPES, and supplemented with 10% of fetal bovine serum, 0.5% of 200 m*M* L-glutamine, and 1% of penicillin/streptomycin solution 100 U/mL each.

The discs of the experimental materials and positive control were incubated in 5 mL of culture medium at (37 ± 1)°C on a roller mixer. The culture medium, containing the soluble extracts from the test materials, was removed after 1 day and replaced by a fresh portion. The procedure was repeated after 2 and 7 days from the starting of the experiment. All the extracts were obtained under sterile conditions and frozen. The cells suspended in culture medium (1.1×10^5 cells/mL) were seeded in 96-well plates (100 μL/well) and incubated for 24 h at (37 ± 1)°C. Then, the culture medium was removed and replaced with 100 μL of the soluble extract of each test material, THX, and TTN, and incubated at (37 ± 1)°C for 24 h. A control test was run with 100 μL of culture medium. A stock solution (5 mg/mL) of MTT in warm phosphate-buffered saline was prepared and diluted at 0.5 mg/mL with culture medium. The extracts were removed from the wells and 100 μL of MTT diluted solution were added and incubated at (37 ± 1)°C for 3.5 h. MTT diluted solution was removed and 100 μL of dimethyl sulfoxide was added and shaken for 20 s, so as to breakdown the cell membrane and to dissolve the dark blue formazan crystals formed inside the viable cells. As blank, a test without material extract or seeded cells was run. The optical density (OD) was measured with a Biotek ELX808IU detector using a test wavelength of 570 nm and a reference wavelength of 630 nm. The values of OD were corrected for the mean absorbance of blank. In all cases the number of replica was 16.

Direct cytotoxicity by the Alamar Blue method

For direct cytotoxicity assay (Alamar Blue method), discs of each material (10 mm diameter × 1 mm thickness), fabricated by isostatic pressing and sintering, were sterilized by ethylene oxide and submitted to direct cytotoxicity test by the Alamar Blue method.[25] The sterile materials and THX as negative control were placed in 24-well plates ($n = 4$) and 1 mL of a cell suspension in complete MEM (1.4×10^5 cells/mL), prepared from a primary culture of human fibroblasts, was added to each well. After incubating at 37 ± 1°C for 1 day, the medium and supernatant cells were removed. One milliliter of Alamar Blue solution, prepared by 1:10 dilution of Alamar Blue solution, Serotec, BUFO12A, with complete MEM without phenol red, was added and plates were incubated for 4 h at (37 ± 1)°C. A blank test was run in the same way, but without using any material and replacing cell suspension by 1 mL of Alamar Blue solution. Four aliquots of 100 μL were extracted from each well and trespassed to a 96-well plate. In all cases, the final number of replica was 16. The wells with the testing materials were washed with phosphate-buffered saline and 1 mL of fresh complete MEM was added and incubation at (37 ± 1)°C was continued to the next reading time, and the procedure repeated. The OD was measured as previously described for MTT assay. Readings were taken at 1, 2, 4, 7, 14, and 21 days from the seeding of cells. The values of absorbance were corrected for the mean absorbance of blank.

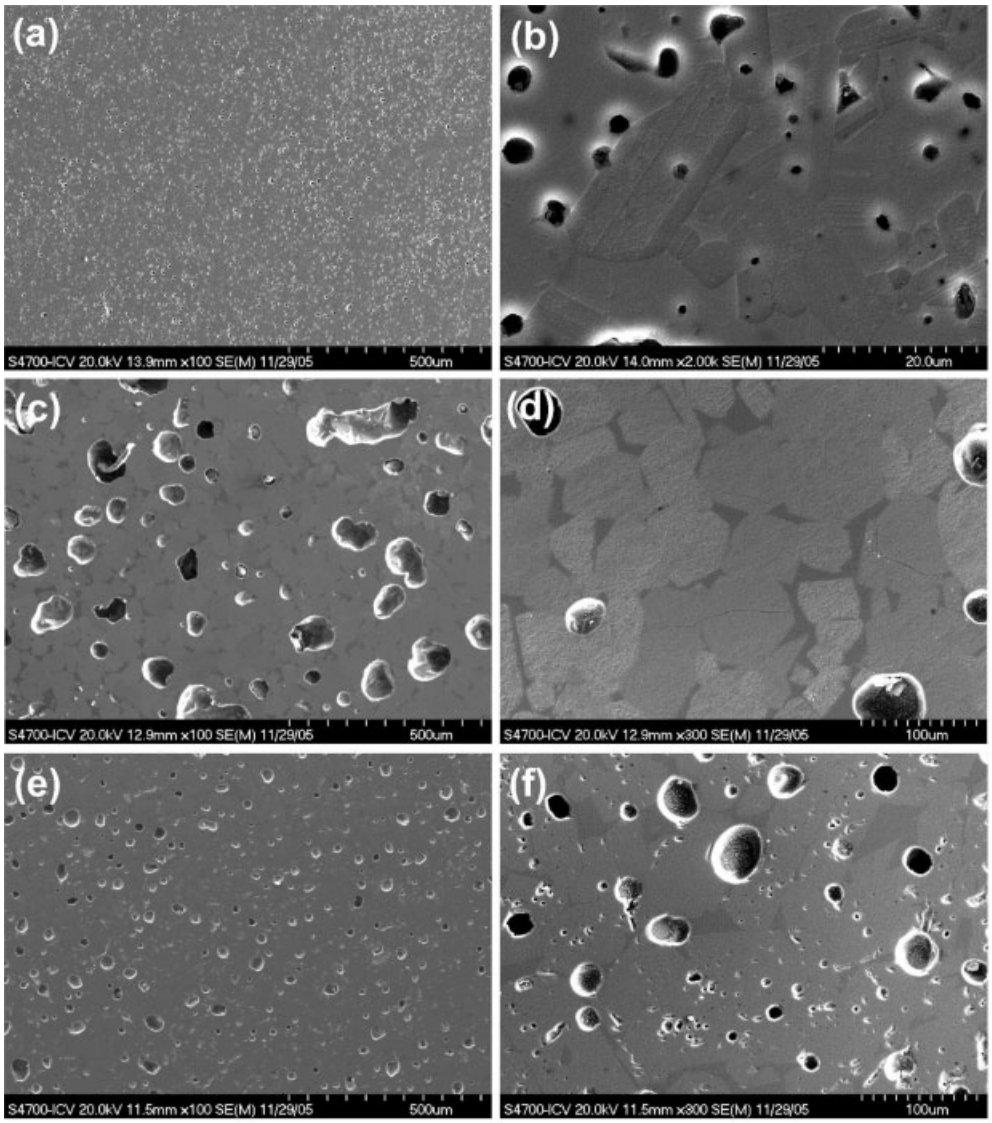

Figure 4. SEM images of the polished surfaces of the sintered samples. (a,b) SSW etched with 1:5 HAc for 2 s; (c,d) SNW no-etched; (e,f) SNW-M no-etched.

Statistics

The statistical analysis of the results was performed under Statistica for Windows (StatSoft, 1999). In all statistical hypothesis tests a confidence level of $\alpha = 0.05$ was considered.

RESULTS

Phase composition and microstructure

Pseudowollastonite (β-$CaSiO_3$, JCPDF 31-0300), the high temperature form of wollastonite, was the only crystalline phase detected by X-ray diffraction in SSW as previously reported [Fig. 3(a)].[8]

The wollastonite-Tc, the main crystalline phase initially present in the natural powder, transformed into pseudowollastonite during sintering, resulting in the same crystalline phase composition in SNW and SNW-M as in SSW [Fig. 3(b)].

However, polished sections of the sintered materials exhibited significant microstructural differences, mainly in pseudowollastonite crystal sizes and in the amount and distribution of the glassy phase (Fig. 4). SSW [Fig. 4(a,b)] presented smaller grain size, lesser amount of intergranular glassy phase, and smaller and more disperse pores than SNW [Fig. 4(c,d)]. By grinding the starting natural powder to reduce its particle size from 13.2 to 2.0 μm, reduction in pore and grain size, the first more accented, were reached in the SNW-M. A more homogeneous distribution of intergranular glassy phase was also observed [Fig. 4(e,f)].

The results of semiquantitative analysis of the glassy phase in the sintered materials, performed by EDS, are shown in Table II. The pseudowollastonite

TABLE II
Results of the Semiquantitative Chemical Analysis of the Glassy Phase

Element (wt %)	SiO_2	CaO	Al_2O_3	Fe_2O_3	MgO	Na_2O	K_2O	Glass
SSW	52	32	8	2	4	1	1	≅2
SNW	51	39	4.5	0.8	7	0.6	–	≅7
SNW-M	57	22	5	3	13	0.9	–	≅15

crystals did not show any evidence of solid solution in any of the samples studied. Therefore, the minor elements in the starting powders were concentrated in the glass formed during sintering of the samples. Consequently, the amount of glassy phase, in all the samples, was roughly estimated from the Al_2O_3 content in the glass, as determined by EDS, and from the Al_2O_3 content in the starting materials, as determined by X-ray fluorescence, corrected for L.O.I. when required (Table I).

Fracture behavior

In Figure 5, characteristic fracture surfaces of the sintered materials are displayed. It was not possible to discern any large defect as obvious fracture origin. At low magnification [Fig. 5(a,c)], fracture was much more tortuous in SNW samples than in the other ones. In the former, large (section ≅ 100 μm) zones surrounded by cracks were observed. Fracture was mostly transgranular in SSW and SNW-M specimens [Fig. 5(d,f)] and mixed transgranular/intergranular in SNW [Fig. 5(b,e)]. In all surfaces, distinguishable pores with sizes obeying the order SNW > SNW-M > SSW were observed.

Characteristic diametral compression strength and Weibull module

The Weibull parameters are summarized in Table III and the diametral compression strength distributions

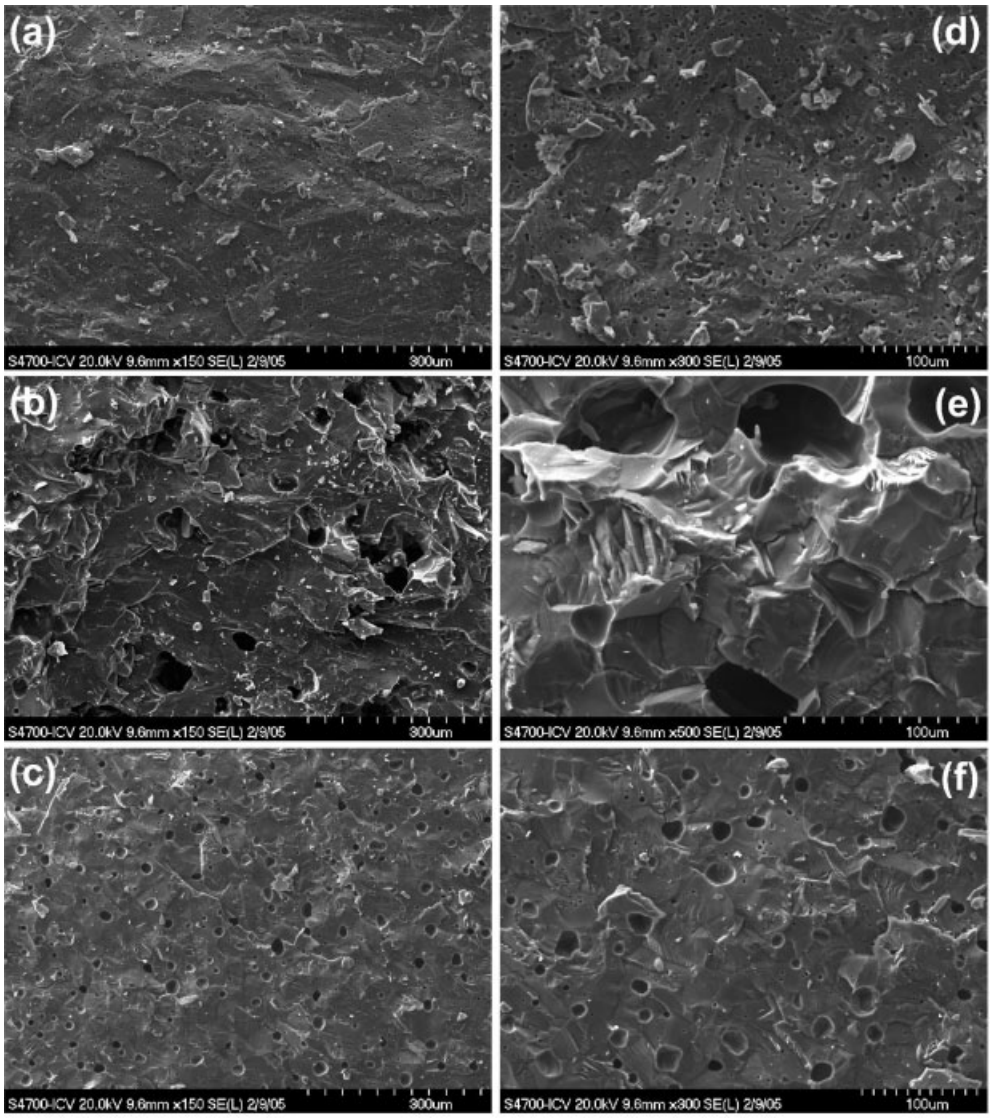

Figure 5. SEM images of the fracture surfaces of the sintered samples: (a,d) SSW; (b,e) SNW; (c,f) SNW-M.

TABLE III
Characteristic Diametral Compression Strength and Weibull Modulus[a]

Material	Weibull Modulus, m		Characteristic Diametral Tensile Strength, σ_0 (MPa)	
SSW	3.52	+1.05	42.17	+6.53
		−1.27		−5.58
SNW	6.47	+1.93	25.55	+2.09
		−2.34		−1.90
SNW-M	7.30	+2.18	48.00	+3.48
		−2.60		−3.16

[a]Upper and lower limits are given for a confidence level of 90%.

calculated from data in Table III are plotted in Figure 6, together with the experimental values for the three studied materials.

Characteristic strength for SNW was, for a confidence level of 90%, significantly lower than for the other two materials, for which no significant differences were found. For Weibull modulus, only significant differences were found for SSW, which was lower than for both SNW materials.

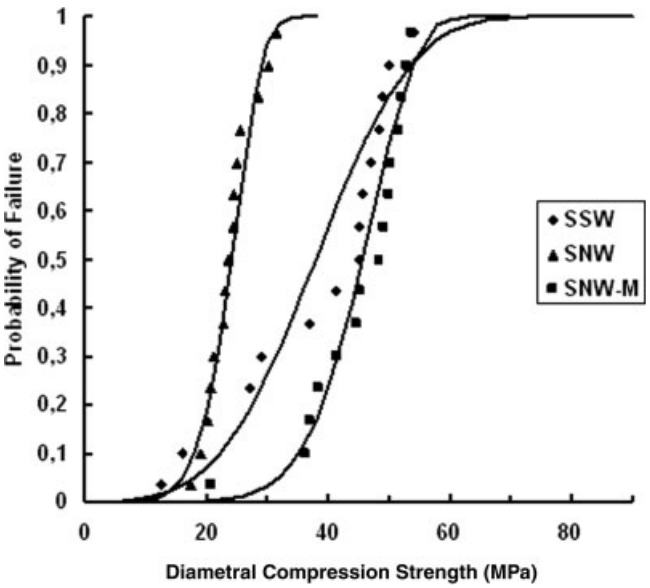

Figure 6. Cumulative distribution for probability of failure versus diametral tensile strength. Symbols correspond to experimental data and solid lines to the Weibull distribution calculated using the values of m and σ_0 of Table III.

Ions release and interfacial pH

The release profiles of Si, Ca, and P ions in SBF at 36.5°C for SSW and SNW are displayed in Figure 7. Both ceramic materials released Si and Ca ions, and removed P ions from SBF in similar way and amounts. The specific concentration of Ca in SBF increased from 100 to 230 mg L^{-1} cm^{-2} when SSW and SNW were incubated at 36.5°C for 504 h (21 days). In addition, SBF was enriched in Si up to a value of 78 mg L^{-1} cm^{-2} for the same incubation period. However, P ions were removed from SBF by both sintered materials, and its concentrations decreased from 31 to 19 and 5 mg L^{-1} cm^{-2} for SSW and SNW, respectively.

The pH at the SBF/ceramic interface continuously increased from a value of 7.4 to over 13.0 after monitoring for 20 h. However, the pH in the SBF bulk solution remained almost steady during the monitoring period (Fig. 8). Exactly the same behavior was observed for SSW and SNW-M.

In vitro bioactivity

The SEM surface images of SSW and SNW after immersion in SBF at 36.5°C for 1 and 3 wk are displayed in Figure 9. The surface of both ceramics were eroded by the dissolution of the wollastonite grains in the SBF during the first periods of immersion and a porous structure, apparently composed of the intergranular vitreous phase, was revealed [Fig. 9(a,c)]. The superficial erosion was quickly followed for the precipitation of globular aggregates of tiny apatite-like crystals that covered the surface of the samples completely. The surface morphologies observed were very similar for all samples and all the immersion periods.

The microanalysis and elemental mapping performed on polished cross-sections of the studied materials after immersion in SBF at 36.5°C for 3 wk rendered the results shown in Figure 10. In both materials an external Ca- and P-rich layer was observed, followed by a Si-rich intermediate layer, coating the pseudowollastonite inner bulk material.

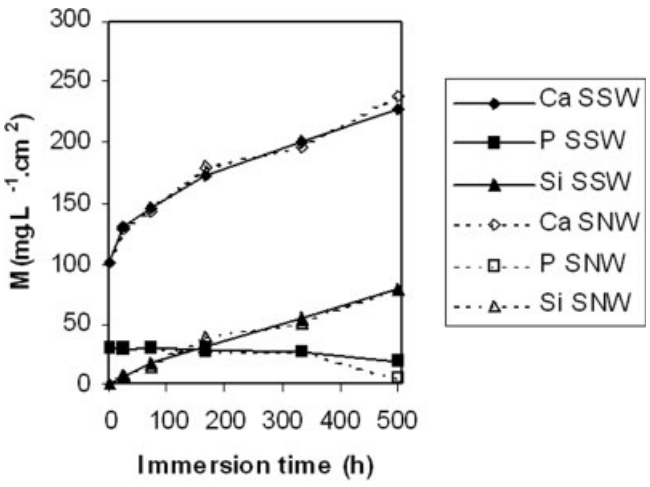

Figure 7. Si, Ca, and P ion release profiles in SBF at 36.5°C.

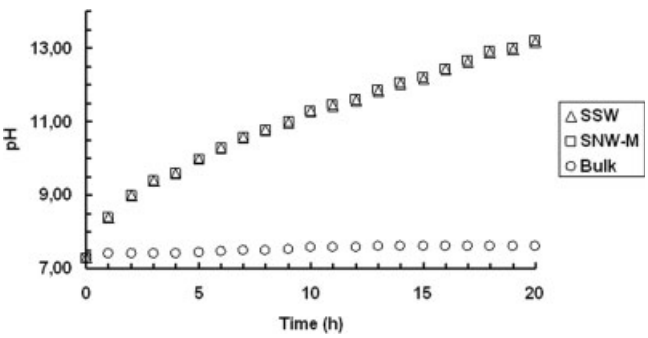

Figure 8. pH evolution at the SBF/ceramic interface and in the bulk solution.

Indirect cytotoxicity

MTT [3-(4,5-dimethylthiazol-2-yl)-2,5-diphenyltetrazolium bromide] assay, first described by Mosmann in 1983, is based on the ability of a mitochondrial dehydrogenase enzyme from viable cells to cleave the tetrazolium rings of the pale yellow MTT and form dark blue formazan crystals which are largely impermeable to cell membranes, thus resulting in its accumulation within healthy cells. The addition of dimethyl sulfoxide results in the disintegration of the cell membrane and the liberation of the crystals which are quickly dissolved. The number of surviving cells is directly proportional to the level of the formazan product created, and the OD of its solution can be measured and related to the amount of viable cells.

MTT assay results obtained for extracts from the experimental materials, THX (noncytotoxic) and TTN (cytotoxic), are displayed in Figure 11. The result for a quality control test is also shown in the figure. The value of O:D obtained for the positive control, TTN, was normal. The OD of the quality control test was also normal but slightly lower than the values of THX for the periods of extraction of 1 and 2 days, according to the T-test for independent samples. At 7 days of extraction there was no significant difference between control and THX, which supported the validity of the method. The ANOVA and post hoc comparison, using the Tukey's honest significant difference test, revealed no significant difference between SNW and SSW for any period of extraction; more else, the extracts from experimental materials and negative control, THX, had no significant difference for periods of extraction of 1 and 2 days, and were significantly less cytotoxic than THX at 7 days of extraction.

Direct cytotoxicity

As employed in this work, Alamar Blue assay was aimed to quantitatively measure cell proliferation,

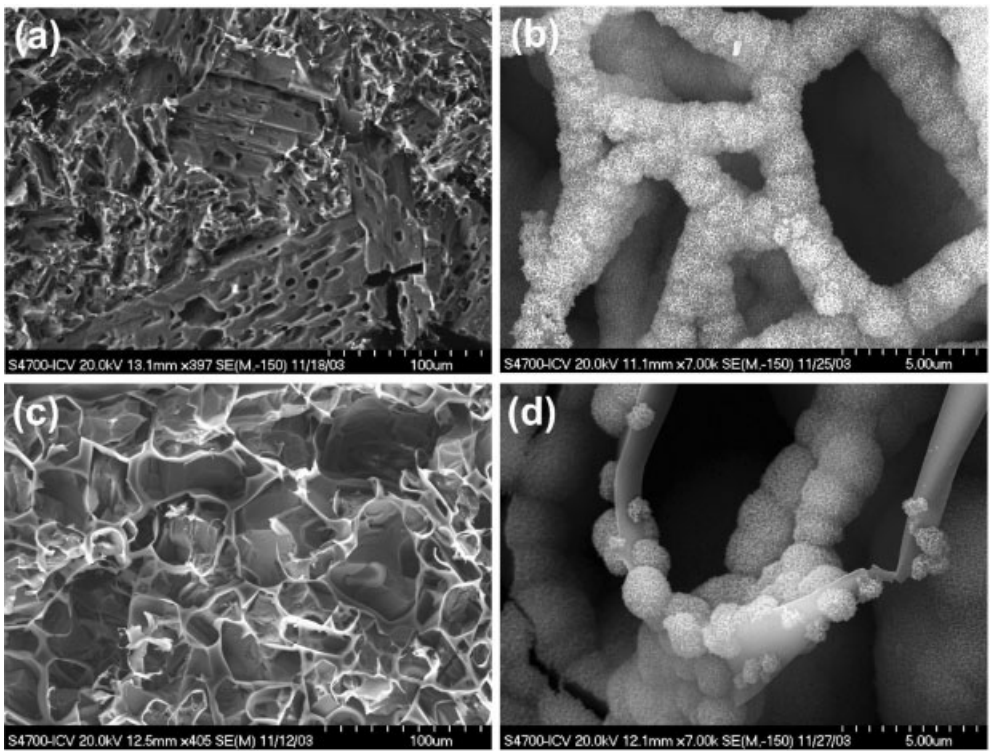

Figure 9. SEM images of the samples surfaces after immersion in SBF at 36.5°C for different periods of time: (a,b) SSW, 1 and 3 wk; (c,d) SNW, 1 and 3 wk.

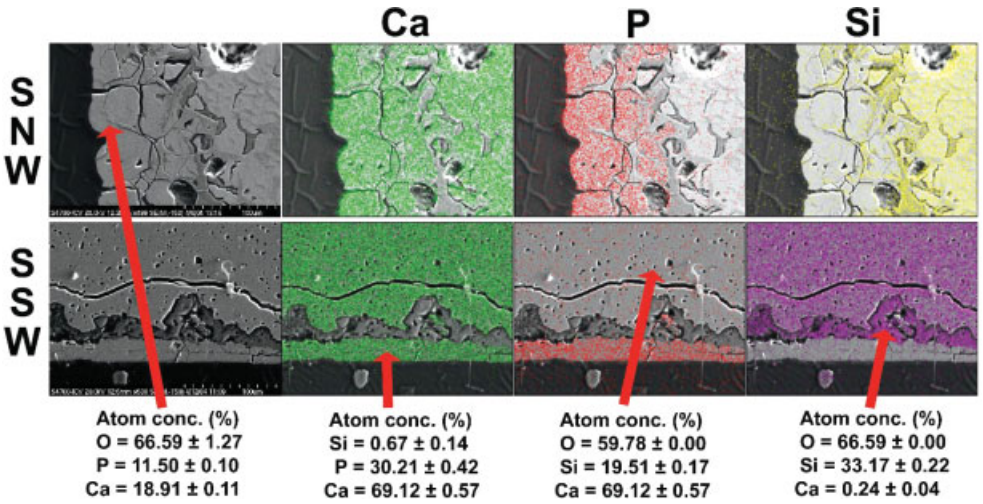

Figure 10. Element mapping and EDS microanalysis of cross-sections of the samples after 3 wk in SBF at 36.5°C. [Color figure can be viewed in the online issue, which is available at www.interscience.wiley.com.]

cytotoxicity, and viability, directly on the materials under study. The method is based on the incorporation of resazurin and resarfurin as colorimetric redox indicators. These indicators respond to chemical reduction resulting from cell metabolism by changing color. This color change may be measured by monitoring the absorbance of the reduced form of the indicator (corrected for the background corresponding to the oxidized form), which is proportional to the amount of viable cells attached to the surface of the tested material.

The results of the Alamar Blue assay performed on the experimental materials and the negative control are represented in Figure 12. Thermanox, the negative control, exhibited higher OD than the experimental materials for all times of culture. The OD corresponding to the experimental materials always reached 80 to 60% of the Thermanox. The ANOVA pointed out significant effects of the material nature, the culture time, and their interaction on OD. There were no significant differences between the ODs of SSW and SNW-M, but both were significantly lower than that of Thermanox for any culture time according to the post hoc comparison of means using the Tukey's honest significant difference test.

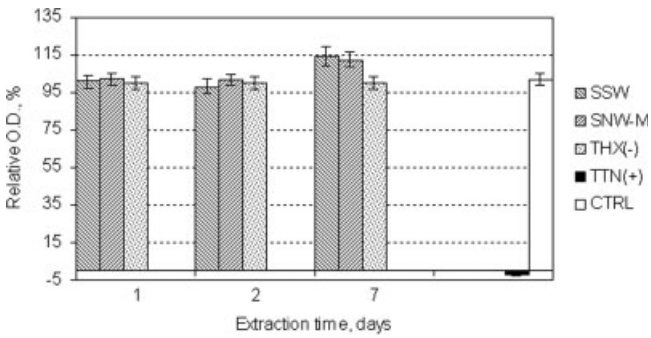

Figure 11. Results of MTT indirect cytotoxicity test. Error bars represent the mean confidence interval ($n = 16$, $\alpha = 0.05$).

DISCUSSION

According to the results of chemical analysis (Table I), both precursor powders had similar amounts of major constituents. However, significant differences were found in the amounts of minor constituents, Al_2O_3, MgO, Na_2O, and Fe_2O_3, which were significantly higher in the natural precursor. They should be related to the minor crystalline phases detected in the natural powder as shown in the X-ray diffractogram of Figure 1(b).

The observed SiO_2/CaO molar ratio in natural wollastonite is slightly grater than the theoretical 1.0 while in synthetic wollastonite is slightly lower (Table I), indicating a slight silica deficiency.

The main crystalline phases in the powders were β-$CaSiO_3$, also called pseudowollastonite, in the synthetic powder and α-$CaSiO_3$ or wollastonite-Tc in the

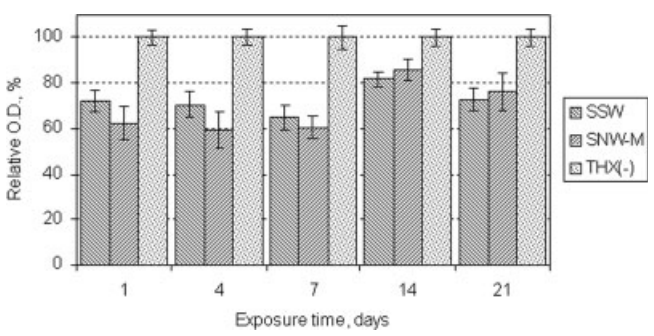

Figure 12. Results of the Alamar Blue test. Error bars represent the mean confidence interval ($n = 16$, $\alpha = 0.05$).

TABLE IV
Young's Modules and Thermal Expansion Coefficients of the Different Phases

Material	Young's Modulus (E) (GPa)	Coefficient of Expansion ($\times 10^{-6}$ C^{-1})
Pseudowollastonite sintered at 1400°C/2 h[27]	94	7.0
Glass in sample SSW	84[a]	6.1[b]
Glass in sample SNW	86[a]	6.3[b]
Glass in sample SNW-M	81[a]	4.5[b]

[a]Calculated according to Navarro[28] and Appen et al.,[29] using the glass composition in Table II.
[b]Calculated assuming ternary SiO_2-CaO-Na_2O glasses, according to Miller and White.[30]

natural one. By heating, over 1125°C, during the sintering, the low temperature form of wollastonite (α-$CaSiO_3$), initially present in the natural powder, transformed reconstructively into β-$CaSiO_3$.[26] At the cooling rate employed in this work, the β→α reversion expected at 1125°C did not take place and the high temperature form was retained at room temperature in both SSW and SNW (Fig. 3).

According to the phase equilibrium diagram of the system CaO-SiO_2,[27] no liquid should exist at the sintering temperature of 1400°C; however, a glassy phase was observed at the grain boundaries in SNW and SNW-M samples and mostly in triple points in SSW as shown in the micrographs of Figure 4. The amount of glassy phase developed in SNW and SNW-M samples was about eight times greater that in SSW (Table II), and it was directly related to the content of impurities in the starting powder (Tables I). The grain size depended on the particle size of the starting powder. The large grains observed in SNW considerably diminished in SNW-M [Fig. 4(e,f)]. A wide grain size distribution was observed in SNW [Fig. 4(c,d)].

In any of the fracture surfaces analyzed there were no large singular defects. The main defects observed in the microstructure of the materials were pores, and sizes were the smallest for material SSW [2–10 μm, Fig. 5(a,d)], intermediate for material SNW-M [20–40 μm, Fig. 5(c,f)], and the largest for material SNW [30–110 μm, Fig. 5(b,e)]. Therefore, large pores should act as critical flaws in the studied materials, and this would explain the lowest values of characteristic strength found for material SNW (Table III), with the largest pore size [Fig. 5(b,e)].

Applying the same approach to SSW and SNW-M, the greatest strength values should be expected for SSW, with the smallest pores [Fig. 5(a–c,f)]. However, the strength values of SSW specimens were similar or even lower than those of SNW-M (Fig. 6) and there were no significant differences between the characteristic strengths of both materials for 90% confidence limits (Table III).

The three studied materials were constituted by a single crystalline phase, pseudowollastonite, and glass. The chemical compositions of the glasses present in the materials (Table II) were close to that of wollastonite. Moreover, negligible residual stresses, due to thermal expansion mismatch, will develop at the boundaries of the two phases (pseudowollastonite and glass), both low Young's modulus[28,29] and thermal coefficients being[30] very similar. (Table IV). Therefore, strong boundaries between the two phases would be expected from a physicochemical standpoint. In fact, fracture was mostly transgranular in specimens SSW and SNW-M [Fig. 5(a,c,d,f)]. In material SNW fracture was mixed trans/intergranular, probably owing to the large glass areas found surrounding some crystalline zones [Fig. 4(c,d)].

The characteristic of the grain boundaries can explain the fact that material SSW, with the finest microstructure [Fig. 4(a,b)], presented lower characteristic strength than did SNW (Fig. 6, Table III). According to Table II, the amount of glassy phase (15 wt %) in SNW-M was considerably larger than in SSW (2 wt %), but it was homogeneously distributed surrounding wollastonite grains [Fig. 4(f)]. Therefore, the higher strength values of SNW-M specimens will be due to the role of the glass acting as effective cement between them. The lowest value of Weibull modulus (Table III) and the bimodal shape of the probability of failure curve observed for SSW (Fig. 6) can be attributed to the small amount of vitreous phase, unevenly distributed in triple points, as well as to a broad distribution of grain sizes [Table II, Fig. 4(b)].

From data in Table III, the best mechanical performance, not only in terms of strength levels but also in terms of reliability, corresponded to the material prepared from natural wollastonite previously milled to a particle size of 2.0 μm (SNW-M).

In the triclinic β-$CaSiO_3$ network, the Ca^{2+} ions are disposed in columns between chains of SiO_4^{4-} tetrahedrons. This special disposition of atoms provides the crystalline network with lability and capability to exchange Ca^{2+} for H_3O^+ ions.[6–9] No differences were noticed in the ion release profiles and interfacial pH (Figs. 7 and 8) for SSW and SNW samples. All materials reacted in the same way and at the same rate when were immersed in SBF at 36.5°C, simulating the body environment. In previous reports, the maximum interfacial pH observed after 20 days in SBF for a synthetic pseudowollastonite ceramic was 10.5.[9] However, in this work, pH values over 13.0 were obtained after 20 h in SBF. The values of pH obtained, apparently unusual, can be due to the lower liquid to area ratio (0.5 cm^3/mm^2) and the experimental assembly here employed.

During the reaction of the ceramics in SBF a fast surface dissolution of pseudowollatonite grains took

place during the first week. The result of the attack was a very porous surface structure constituted by the remainder glassy phase, mainly located at triple points in sample SSW and grain boundaries in SNW [Fig. 9(a,c)]. As the dissolution progressed, the Ca^{2+}, OH^{-}, and PO_4^{3-} activities overcame the solubility product of apatite and this starts to precipitate with the typical morphology of globules constituted by aggregates of very fine acicular crystals [Fig. 9(b,d)].

The mechanism of the formation of the apatite layer on pseudowollatonite was previously described by some of the present authors[6,8,9] and can be summarize in the following steps:

1. Exchange of Ca^{2+}, from the pseudowollastonite network, by H_3O^{+}, from the SBF, and pH increasing at the pseudowollastonite/SBF interface;
2. Formation of a surface layer of hydrated silica gel, which partially dissolves at the high interfacial pH;
3. Increasing of Ca^{2+}, OH^{-}, HPO_4^{2-} ionic activities at the neighborhood of the reacting surface until they overcome the solubility product of the apatite;
4. Nucleation of apatite on the remainder hydrated silica gel layer; and
5. Growing of the apatite nuclei and growing of the apatite layer as well.

This mechanism is common to most of bioactive silicon-containing materials[1,3,9] and was confirmed for SSW and SNW by the results of the elemental mapping and microanalysis performed on polished cross sections of these materials submitted to immersion in SBF for 3 wk (Fig. 10).

In previous reports it has been clearly established that synthetic pseudowollastonite is not cytotoxic, biocompatible, and osteogenic.[10–15] However, no study on the cytotoxicity of pseudowollastonite ceramic obtained from natural precursors has been performed. SNW contain certain impurities that are absent in SSW and could induce a different response on *in vitro* cell cultures. However, the results of the MTT test displayed in Figure 11 demonstrated that the soluble extracts from SNW and SSW exerted the same effect on the culture of human fibroblasts, and both were completely innocuous as evidenced by comparison with the results for the negative control, Thermanox.

From the results of the Alamar Blue test displayed in Figure 12, SNW and SSW exhibited the same behavior again. However, the cell adhesion on SSW and SNW were significantly lower than on the negative control, Thermanox. This situation may be a consequence of the fast surface remodeling that takes place when the materials are immersed in MEM. MEM has an ionic composition and pH similar to SBF; thus, the same surface reactions observed in SBF should occur when the ceramics are immersed in MEM. The fast dissolution of the surface and the local pH increasing prior to the formation of the stable apatite layer could hinder cell adhesion during the first periods of immersion. The formation of the stable apatite layer should provide a more "comfortable" bed to cell adhesion. According to this hypothesis, direct cell adhesion tests on bioactive materials that suffer a fast surface remodeling by immersion in the body environment, as pseudowollastonite, should be better carried out after a previous immersion period in the culture medium to stabilize their surface. The favorable results of *in vivo* tests conducted on synthetic pseudowollastonite ceramics and previously reported[10,11] show that the material is perfectly biocompatible, bioactive, and osteoconductive, in spite of the apparently negative results obtained in the Alamar Blue test conducted in this work.

CONCLUSIONS

According to the obtained results, polycrystalline psedowollastonite ceramics properly processed, from pure powder precursors of natural origin, exhibited chemical and phase compositions, *in vitro* reactivity, bioactivity, and cytotoxicity very similar to those of pseudowollastonite ceramic obtained by the synthetic route, and even better performance, in terms of strength and reliability, than the more expensive synthetic material.

The results support the safe and successful use, in biomedical applications, of pseudowollastonite bioceramics obtained from pure natural precursors.

References

1. Hench LL, Splinter RJ, Allen WC, Geenle TK. Bonding mechanisms at the interface of ceramic prosthetic materials. J Biomed Mater Res 1972;2:1117–1141.
2. Kokubo T, Ito S, Sakka S, Yamamuro T. Formation of high-strength bioactive glass-ceramic in the system MgO-CaO-SiO_2-P_2O_5. J Mater Sci 1986;21:536–540.
3. Hench LL, Wilson J, editors. An Introduction to Ceramics. Advanced Series in Ceramics, Vol. 1. Singapore: World Scientific; 1993.
4. Ohura K, Nakamura T, Yamamuro T, Kokubo T, Ebisawa T, Kotoura T. Bone bonding ability of P_2O_5-free CaO-SiO_2 glasses. J Biomed Mater Res 1991;25:357–365.
5. Nonami T, Tsutsumi S. Study of diopside ceramics for biomaterials. J Mater Sci Mater Med 1999;10:475–479.
6. De Aza PN, Guitian F, De Aza S. Bioactivity of wollastonite ceramics: In vitro evaluation. Scr Metall Mater 1994;31:1001–1005.
7. De Aza PN, Lublinska ZB, Anseau MR, Guitián F, De Aza S. Bioactivity of pseudowollastonite in human saliva. J Dent 1999;27:107–113.
8. De Aza PN, Lublinska ZB, Anseau M, Guitián F, De Aza S. Morphological studies of pseudowollastonite for biomedical applications. J Microsc 1996;182(Pt. 1):24–31.
9. De Aza PN, Guitian F, Merlos A, Lora-Tamayo E, De Aza S. Bioceramics-simulated body fluid interfaces: pH and its influ-

ence on hydroxyapatite formation. J Mater Sci Mater Med 1996;7:399–402.
10. De Aza PN, Lublinska ZB, Martinez A, Anseau MR, Guitián F, De Aza S. Morphological and structural study of pseudowollastonite implants in bone. J Microsc 2000;197(Pt. 1):60–67.
11. De Aza PN, Luklinska ZB, Anseau MR, Guitián F, De Aza S. Transmission electron microscopy of the interface between bone and pseudowollastonite implant. J Microsc 2001;201(Pt. 1):33–43.
12. Dufrane D, Delloye C, Mckay IJ, De Aza PN, De Aza S, Schneider YJ, Anseau M. Indirect cytotoxicity evaluation of pseudowollastonite. J Mater Sci Mater Med 2003;14:33–38.
13. Sarmento C, Luklinska ZB, Brown L, Anseau M, De Aza PN, De Aza S, Hughes FJ, McKay IJ. The in vitro behaviour of osteoblastic cell cultured in the presence of pseudowollastonite ceramic. J Biomed Mater Res 2004;69A:351–358.
14. Brown L, Lublinska ZB, De Aza PN, De Aza S, Anseau M, Hughes FJ, McKay IJ. Proceedings of the 7th World Biomaterials Congress, Sydney, Australia, May 17–21 (2004).
15. Brown L, Lublinska ZB, De Aza PN, De Aza S, Anseau M, Hughes FJ, McKay IJ. Silicon released from bioactive ceramic materials enhances osteoblastic differentiation. Biomaterials. Submitted for publication.
16. O'Driscoll M. Wollastonite. Ceramics remains top consumer. I.M. Glass & Ceramics Survey. Ind Minerals 1993 (Special Issue):77–83.
17. De Aza PN, Guitián F, De Aza S, Valle FJ. Analytical control of wollastonite for biomedical applications by use of atomic absorption spectrometry and inductively coupled plasma atomic emission spectrometry. Analyst 1998;123:681–685.
18. Kim H-M, Miyazaki T, Kokubo T, Nakamura T. Revised simulated body fluid. Key Eng Mater 2001;192–195:47–50.
19. Carneiro FLLB, Barcellos A. Résistance à la traction des bétons. Bull RILEM(I) 1953;13:97–108.
20. Rudnick A, Hunter AR, Holden FC. An Analysis of the Diametral-Compression Test. Mater Res Stand 1963;4:283–289.
21. Villora JM, Callejas P, Barba MF, Baudín C. Statistical analysis of the fracture behaviour of porous ceramic raschig rings. J Eur Cer Soc 2004;24:589–594.
22. Weibull W. A statistical distribution function of wide applicability. J Appl Mech 1951;18:292–297.
23. Ferrari B, González S, Moreno R, Baudín C. Strength analysis of self-supported films produced by aqueous electrophoretic deposition. J Am Cer Soc 2005;88:2645–2648.
24. Mosmann T. Rapid colorimetric assay for cellular growth and survival: Application to proliferation and cytotoxicity assays. J Immunol Methods 1983;65:55–63.
25. Nakayama GR, Caton MC, Nova MP, Parandoosh Z. J Immunol Methods 1997;204:205–208.
26. Deer WA, Howie RA, Zussman J. Rock Forming Minerals, 2nd ed. Vol. 2A. Single-Chain Silicates. London: Longmans; 1978. p 547–563.
27. Phillips B, Muan A. Phase equilibria in the system CaO–iron oxide–SiO_2, in air. J Am Ceram Soc 1959;42:413–423.
28. Fernández Navarro JM. El Vidrio. Madrid: Sociedad Española de Cerámica y Vidrio; 1993.
29. Appen AA, Kozlovskaya EI, Fu-Si H. Study of the elastic and acoustic properties of silicates glasses. J Appl Chem (U.S.S.R.) 1961;34:975–981.
30. Miller GH, White D. Composition-thermal expansion relationships in ternary glass systems. Glass Technol 1977;18: 113–116.